arXiv:2508.18486v2 [physics.ao-ph] 24 Jun 2026

Huracan: A Skillful End-To-End Data-Driven System for Ensemble Data Assimilation and Weather Prediction

Zekun Ni[1*], Jonathan Weyn[1], Hang Zhang[1], Yanfei Xiang[2†], Jiang Bian[1], Weixin Jin[1], Kit Thambiratnam[1], Qi Zhang[1], Haiyu Dong[1], Hongyu Sun[1]

[1]Microsoft Corporation.
[2]Department of Earth System Science, Ministry of Education Key Laboratory for Earth System Modeling, Institute for Global Change Studies, Tsinghua University, Beijing, China.

*Corresponding author(s). E-mail(s): zekunni@microsoft.com;
†Work done while at Microsoft Corporation.

Abstract

Over the past few years, machine learning-based data-driven weather prediction has been transforming operational weather forecasting by providing more accurate forecasts while using a mere fraction of computing power compared to traditional numerical weather prediction (NWP). However, those models still rely on initial conditions from NWP, putting an upper limit on their forecast abilities. A few end-to-end systems have since been proposed, but they have yet to match the forecast skill of state-of-the-art NWP competitors. In this work, we propose Huracan, an observation-driven weather forecasting system which combines an ensemble data assimilation model with a forecast model to produce highly accurate forecasts relying only on observations as inputs. Huracan is not only the first to provide ensemble initial conditions and end-to-end ensemble weather forecasts, but also the first end-to-end system to achieve an accuracy comparable with that of ECMWF ENS, the state-of-the-art NWP competitor, despite using a smaller amount of available observation data. Notably, Huracan matches or exceeds the continuous ranked probability score of ECMWF ENS on 80.2% of the variable and lead time combinations. Our work is a major step forward in end-to-end data-driven weather prediction and opens up opportunities for further improving and revolutionizing operational weather forecasting.

Keywords: Machine learning, ensemble weather forecasting, data assimilation

1 Introduction

Operational weather forecasting has traditionally relied on a backbone of global numerical weather prediction (NWP). NWP systems consist of two components: data assimilation (DA) and the forecasting model. At each issue time, observation data newly produced after the last cycle are ingested into the data assimilation system, which combines them with the initial guesses – forecasts from the last cycle – to produce initial conditions for this new cycle. The forecasting model then uses physics-based numerical methods to generate forecasts based on these initial conditions. This system is not only immensely heavy in computation, requiring specialized supercomputers to run, but also inherently complex as it runs through a variety of steps involving both well-sounded physical and statistical equations as well as empirical parameterizations.

Over the past few years, machine learning- (ML) based data-driven weather prediction methods have offered a viable alternative to traditional NWP, providing more accurate forecasts while using a small fraction of computational power. This area was first explored by Weyn et al [1]. Within a few years of advancement, Pangu-Weather [2] and GraphCast [3] became the first data-driven models to comprehensively outperform the best deterministic NWP forecasts. Shortly thereafter, ensemble forecasting models such as GenCast [4] and AIFS-CRPS [5] showed that data-driven methods could also succeed at probabilistic forecasting.

Despite these breakthroughs, all operational ML-based models are still initialized with NWP-derived initial conditions such as those from ECMWF HRES and ENS. The data assimilation component has seen slower adoption of ML techniques. A few end-to-end data-driven DA systems have been proposed, such as Aardvark [6], FuXi Weather [7] and GraphDOP [8], but none of them has so far been able to match the forecast skill of state-of-the-art NWP competitors when coupled with a weather prediction model, highlighting the challenging nature of this problem. Overcoming these challenges could yield high rewards: Most of the forecast uncertainty comes from the initial conditions, not the forecasting model [9, 10]. Therefore, any progress on data assimilation may bring much bigger impact on forecast skill compared to improvements on the forecasting model. NWP DA systems are complicated by many processes including quality control, observation operators, error and covariance estimation, linear tangent physics and bias correction [11, 12]; it's reasonable to believe ML-based data-driven methods may be able to tackle these effectively.

In this paper, we present Huracan, a skillful end-to-end data-driven system consisting of both ensemble data assimilation and ensemble weather prediction. Unlike previous works, Huracan is the first to provide ensemble initial conditions, therefore completing the whole operational system with uncertainty estimates. At 1-degree resolution, our coupled system is able to provide ensemble weather forecasts for up to 10 days on a set of atmospheric variables including temperature, humidity, geopotential

and wind at 13 pressure levels as well as surface-level temperature, wind and cloud cover. Using the widely accepted continuous ranked probability score (CRPS) metric for evaluation, forecasts provided by Huracan are as good (within 2% difference) or better than those from the state-of-the-art NWP system, ECMWF ENS, on 559 of the 697 (80.2%) lead time and variable combinations, when evaluating against each model's own analysis. Even when comparing with the strongest baseline so far, which uses a hybrid approach of ECMWF ENS initial conditions and ML-based forecasts, our end-to-end forecasts are still as good or better on 65.1% of the combinations. To the best of our knowledge, this is the first time that an end-to-end data-driven system can rival a whole NWP system while providing equally good initial conditions and forecasts in mere minutes after all observations arrive.

2 Methods

2.1 Data

The essential part of a data assimilation system is the observations. As is commonly used in NWP [13] and previous ML-based DA models, we include level-1 observations from microwave and hyperspectral infrared sounders onboard the Metop, NOAA and JPSS satellites, level-2 bending angle profiles from GNSS-RO radio occultations, level-1 visible and infrared radiances from geostationary satellites as well as in-situ observations from land-based weather stations and radiosondes. According to diagnostics from NWP [14, 15], we have included the observation types that contribute most to forecast skill, but have still omitted some other potentially impactful sources such as scatterometers or flight winds. Table 1 summarizes the observations we are using in Huracan. Our training set spans over years 2010 through 2022, while years 2023 and 2024 are reserved for validation and testing, respectively.

An inherent challenge associated with observation data is that, unlike analyses or initial conditions, observations are much more "ill-behaved" in that they can be sparse, don't necessarily align with certain grid points or time boundaries, and can have quality issues. Below we briefly outline the steps we take to process different kinds of observation data:

1. Simple quality control is carried out, which includes removing data with bad quality flags or physically implausible values (brightness temperature < 100 K or > 400 K).
2. Hyperspectral infrared and radio occultation data are processed into unified formats and compressed by autoencoders into 32 and 64 channels, respectively. Implementation of the autoencoders is outlined in Section A.1.
3. Level 1 satellite observations are first bilinearly interpolated to a higher-resolution intermediate grid from their native coordinates. All gridded satellite data, along with the already gridded GridSat datasets, are then conservatively interpolated to the final 1-degree resolution. Sparse in-situ observations and radio occultation embeddings are directly assigned to the closest grid point, with multiple observations being averaged at the same grid point.
4. Satellite channels with similar nominal frequencies are merged into one, and all observations are grouped into equally-spaced time frames. Only the observations

Table 1: Data sources used in Huracan.

Category	Instrument	Period	Format/Dataset
Microwave Sounders	NOAA 15–19 AMSU-A	2010-2024	Level 1b [16]
	Metop A–C AMSU-A	2010-2024	Level 1b [17]
	Aqua AMSU-A	2010-2024	Level 1b [18]
	NOAA 15–17 AMSU-B	2010-2014	Level 1b [16]
	NOAA 18, 19 MHS	2010-2024	Level 1b [16]
	Metop A–C MHS	2010-2024	Level 1b [19]
	S-NPP, NOAA 20, 21 ATMS	2011-2024	Level 1b [20–22]
Hyperspectral IR Sounders	Metop A–C IASI	2013-2024	Level 1c [23]
	S-NPP, NOAA 20, 21 CrIS	2012-2024	Level 1b [24–27]
	Aqua AIRS	2010-2024	Level 1b [28]
Radio Occultation	GNSS-RO	2010-2024	Level 2 [29]
Geostationary Imagers	GOES 16–19 ABI	2017-2024	Level 1b [30]
	Himawari 8, 9 AHI	2015-2024	Level 1b [31]
	Meteosat 8–11 SEVIRI	2010-2024	Level 1.5 [32]
	Meteosat 8, 9 IODC SEVIRI	2017-2024	Level 1.5 [33]
	GOES 11–15 IMAGER	2010-2017	GridSat-GOES [34]
	Global satellite composites	2010-2017	GridSat-B1 [35]
In-situ Observations	Radiosondes	2010-2024	IGRA [36]
	Land-based stations	2010-2024	ISD [37]

closest to the frame boundaries are used. Metadata including satellite viewing angles and time differences between the observations and frame boundaries are added as extra channels.

5. After normalization, grid points without any available observations are assigned to zero.

Apart from observation data, we also utilize the ERA5 [38] dataset for ground truth as well as background initial conditions. Huracan assimilates and predicts 72 variables, including 5 upper-air variables across 13 pressure levels and 7 surface variables. The full list of all model variables and input-only observation channels is provided in Table 2. Samples of some observation channels are shown in Figure 1.

2.2 Architecture

Huracan consists of two separate models for the data assimilation and forecasting tasks, but they share the identical architecture apart from the number of input channels to the encoder. The overall architecture is based on the Spherical Fourier Neural Operator (SFNO) network [39], with the following substantial modifications:

- In the SFNO blocks, one multi-layer perceptron (MLP) is replaced by a Swin Transformer [40] block. This idea takes its root in the work of Kunyu [41], and has drastically improved the modeling capability of the whole network and resulted in greatly improved performance in practice. The structure of each modified SFNO block is outlined in Figure 2.

Table 2: **Model variables and observation channels per time step used in Huracan.**

Type	#Channels	Description
Model Variables	65	Atmospheric variables: z, t, u, v, q on 13 levels
	7	Surface variables: 2t, 2d, 10u, 10v, tcc, tcwv, msl
Input-only Variables	1	Insolation
	2	Constants: z, lsm
Observations	6×11	SEVIRI channels 1-11, hourly[1]
	2×23	ATMS channels 1-22 & MHS channel 1, 3-hourly[1]
	2×32	32 hyperspectral IR embeddings, 3-hourly
	64	64 radio occultation embeddings
	65	In-situ observations of atmospheric variables
	6	In-situ observations of surface variables except tcwv
	6×1	Zenith angle of the geostationary imager
	2×4	Zenith angles of MW and IR sounder instruments[2]
	2×4	Time differences of MW and IR sounder observations[2]
	1	Time difference of radio occultation profiles

[1] Includes matching channels from other instruments and/or datasets.
[2] One channel per time frame for each of the AMSU-A, AMSU-B/MHS, ATMS and hyperspectral IR instruments.

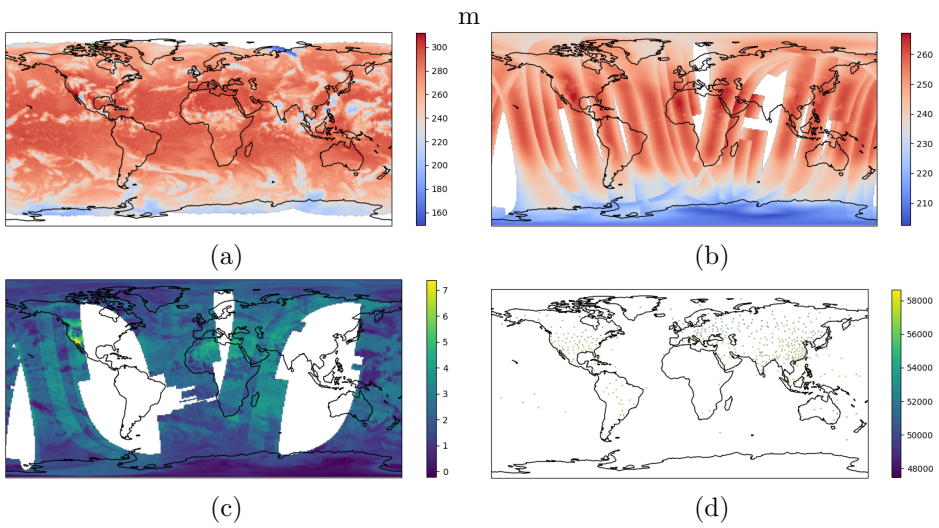

Fig. 1: **Samples of observation data used in Huracan.** (a) SEVIRI Channel 9 (ABI & AHI Channel 14) brightness temperature; (b) ATMS Channel 6 (AMSU-A Channel 5) brightness temperature; (c) Hyperspectral IR Embedding Channel 1 between 21 UTC, August 8, 2019 and 0 UTC, August 9, 2019; (d) in-situ observation of 500 hPa geopotential at 0 UTC on August 9, 2019.

- We have aggressively compressed the filter weights in the SFNO blocks, reducing the number of parameters 12-fold. Such compression mitigates the tendency of overfitting, and is detailed in Section A.2.
- Similar to AIFS-CRPS [5], in anticipation of stochasticity, noise embeddings are generated from random Gaussian noise through a MLP processor. These noise embeddings serve as the context embedding for each grid point and are passed into conditional layer normalizations [42], replacing the existing standard layer normalizations.

Both the assimilation and forecasting models take two time steps $(T_0 - 6\text{h}, T_0)$ as input and predict two time steps in the future $(T_0 + 6\text{h}, T_0 + 12\text{h})$, while internally the time dimension is removed by flattening the input. Such configuration stabilizes autoregressive inference and reduces the number of autoregressive steps in rollout finetunes. Besides 72 model variables for each time step, three forcing and constant variables are added to the input, and the assimilation model additionally receives 269 channels per time step, representing all observations taking place during the past 6 hours before that time step, as shown in Table 2. In this sense, the assimilation model should actually be characterized as a forecasting model with assimilation added on top.

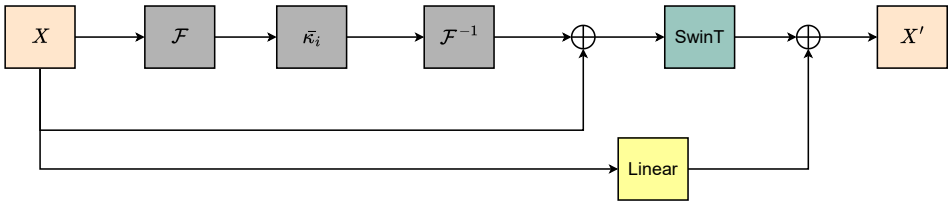

Fig. 2: **The architecture of a modified SFNO block in Huracan.** The most notable change is the replacement of a MLP block by a Swin Transformer block.

2.3 Training

The whole training process consists of multiple phases. At first, a *deterministic base* model is trained using 36 years of ERA5 data under L1 loss, much like every other deterministic ML-based model. This base model is then fine-tuned with the addition of noise and a change to the CRPS as the training objective. This *stochastic base* model is then further fine-tuned to produce the assimilation and forecasting models:

- The *initial forecasting* model is produced by undergoing a 6-step autoregressive fine-tune, which means a maximum rollout window of 3 days.
- The *initial assimilation* model is initialized with weights from the stochastic base model except for the new columns in the encoder corresponding to the observation channels, which are randomly initialized. This model is then fine-tuned using an 8-step autoregressive scheme with the initial condition and the ground truth of each step coming from ERA5 and the observation channels coming from the 15-year

data mentioned above. The long rollout window of 4 days coincides with the time estimated to take for old background errors to become negligible [43], and ensures the model makes the best use of the observations instead of relying heavily on the initial background from ERA5.

Finally, both models are fine-tuned together under a process consisting of 8 autoregressive assimilation steps and 8 forecasting steps. This produces the final ensemble assimilation and forecasting models which make up our Huracan system.

Additionally, a strong baseline forecasting model is trained by fine-tuning the initial forecasting model over ECMWF analysis. This model is then inferenced with ensemble initial conditions from ECMWF ENS to produce a hybrid baseline more skillful than ECMWF ENS forecasts. We dub this system Huracan-Hybrid.

3 Results

3.1 Forecast Skill

In this section, we select 100 issue times in the test year of 2024 from January 1 to December 17, when hindcasts from ECMWF are available, and compare CRPS scores from three ensemble forecasts over 10 lead days: ECMWF ENS, Huracan-Hybrid and the end-to-end Huracan, evaluated against each other's analysis.

Regarding Huracan, we run 48 independent ensemble data assimilation (EDA) members with each member initialized from the same initial condition provided by ERA5 at 0 UTC on October 1, 2023. Even though the ultimate initial condition comes from NWP, it should have a negligible impact over our performance after at least three months of data assimilation. The "analysis" chosen for Huracan is the ensemble mean of the 48 EDA members, in consistent with the practice in NWP systems. Regarding ECMWF ENS, the initial conditions, forecasts and analyses are conservatively downsampled to 1-degree to match the resolution of Huracan and Huracan-Hybrid.

We adopt the notation of skill scores proposed in Graphcast [3] and display the scorecards of CRPS skill scores in Figures 3 and 4 comparing Huracan versus ECMWF ENS, and Huracan versus Huracan-Hybrid.

We can conclude from the scorecards that Huracan generally shows good forecast skill especially compared with ECMWF ENS, while there are some variations between different variables and levels. Huracan performs better on humidity and temperature than on geopotential and pressure, and is slightly more skillful on upper, lower troposphere (200, 850 hPa) and surface compared to mid-troposphere (500 hPa). In comparison with ECMWF ENS, after removing the noisy first two steps due to initial higher spread in our ensemble, Huracan mostly has improved metrics on temperature and humidity but is slightly behind on geopotential. However, when the baseline switches to the stronger Huracan-Hybrid, there is more degradation in geopotential and pressure while Huracan still generally outperforms or matches Huracan-Hybrid on temperature, humidity and wind.

To paint a more complete picture of the three ensembles, Figure 5 shows line charts of CRPS and ensemble spread-skill ratio (ESSR) metrics of the three ensembles for three key variables. Huracan has interesting behavior in ESSR, showing higher spread

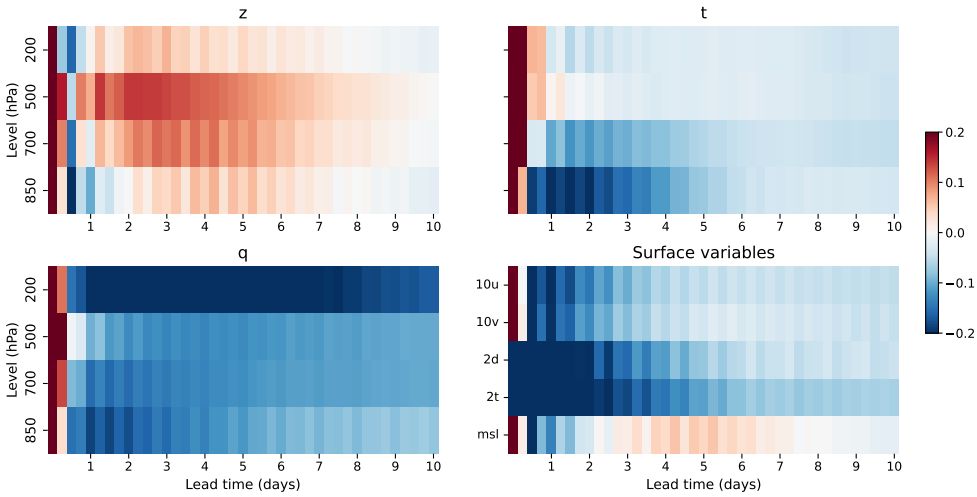

Fig. 3: **Scorecard comparing CRPS scores of Huracan versus ECMWF.** Colors are based on skill scores, which are relative differences in CRPS forecast skill. Blue colors mark improvements and red colors stand for degradations. Evaluations are carried out on geopotential (z), temperature (t) and specific humidity (q) at four vertical levels (200, 500, 700, 850 hPa) as well as 5 surface variables 2m temperature (2t), 2m dewpoint temperature (2d), 10m u and v components of wind (10u, 10v) and mean sea level pressure (msl).

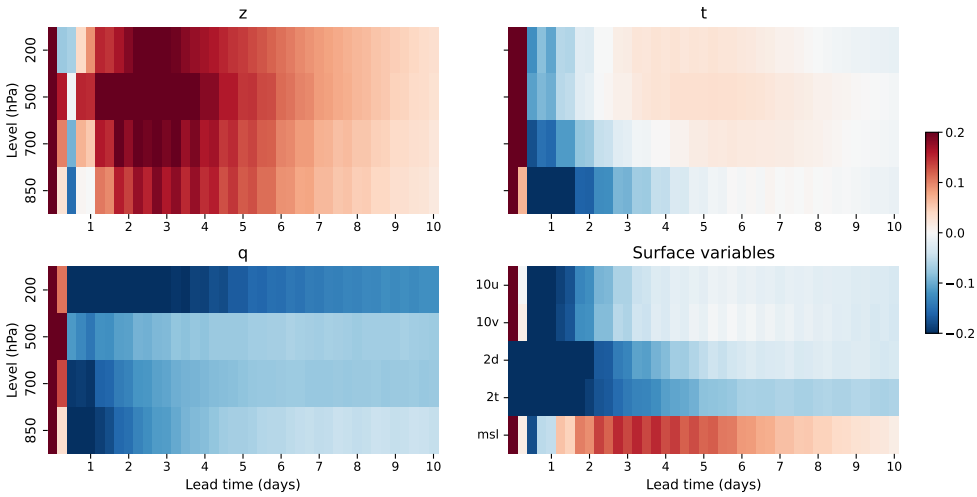

Fig. 4: **Scorecard comparing CRPS scores of Huracan versus Huracan-Hybrid.** Like Figure 3, colors are based on skill scores. Blue colors mark improvements and red colors stand for degradations.

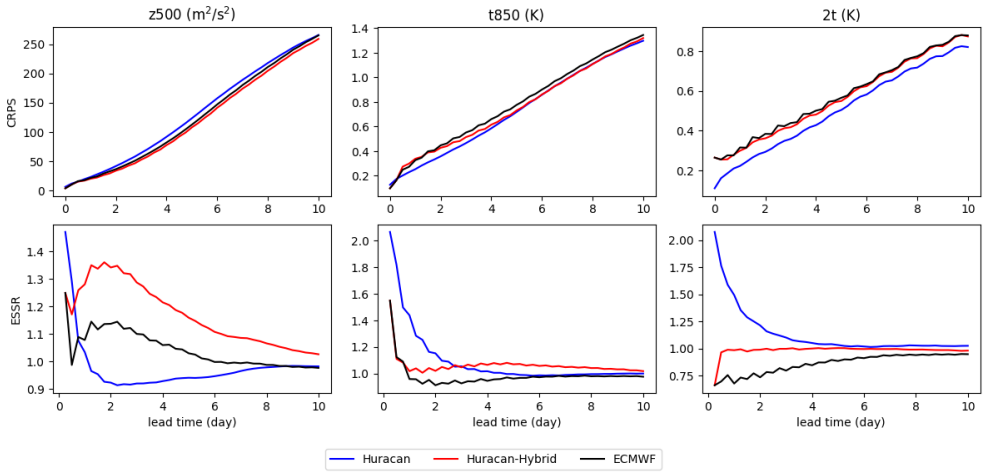

Fig. 5: **Line charts detailing ensemble metrics of Huracan, Huracan-Hybrid and ECMWF ENS.** Charts shown above are CRPS and ESSR metrics for three key variables: 500 hPa geopotential (z500), 850 hPa temperature (t850) and 2m temperature (2t).

at the beginning but lower spread around 3–5 lead days. The initial higher spread should be explained by differences in methodology. in ECMWF ENS, ensemble members are generated from perturbing the deterministic control member [44], while in Huracan, no such member exists and all members are run independently. Therefore, even though both analyses are ensemble mean, our analysis is closer to the true expectation value, therefore the larger ESSR. The likely cause of the later lower spread is overfitting, as similar evaluation results in a training year have ESSR consistently above 1 throughout the 10 lead days.

3.2 Visualization

We additionally visualize the mean and standard deviation of Huracan ensemble members at 0 UTC on October 3, 2024 in Figure 6, in comparison with those from ECMWF ENS initial conditions.

The ensemble mean values generally agree well between Huracan and ECMWF ENS, mostly showing the same large-scale patterns, with small disagreements in details. At the same time, our ensemble mean values are slightly more smoothed, due to the differences in methodology explained above. The lower native resolution of ERA5, which Huracan is trained to predict, could also play a role, especially in the case of the Atlantic Hurricane Kirk, clearly featured in both maps.

Similar differences exist in the ensemble standard deviation values. Although both perturbations display similar patterns, our perturbations are slightly larger in general and are more spread out, while those from ECMWF ENS are more concentrated, with more extreme perturbations at a few localized spots.

4 Discussion

Our end-to-end ensemble data assimilation and forecasting system, Huracan, demonstrates impressive medium-range forecast skill for both upper-air atmospheric variables and surface variables. Huracan generally has as good or better metrics for temperature and humidity, no matter if the baseline is ECMWF ENS or the analysis-initialized Huracan-Hybrid. Such a robust result indicates that Huracan can effectively assimilate multiple kinds of observations, including satellite radiances and in-situ observations. Moreover, it's worth mentioning that in the case of ECMWF ENS, a 0 UTC initial condition actually comes after assimilating all observations received by 3 UTC [12]; and as such, it includes future observations that Huracan does not. The most remarkable difference though, is that our assimilation only takes one single model step, orders of magnitude faster than ECMWF ENS.

Our system relatively under-performs on pressure and geopotential. In addition to adding more data sources, there are some other, more interesting means to try improving the model skill. One potential direction is to use a better architecture to handle sparse observations, which is more in line with Aardvark and GraphDOP, rather than assigning them to grid points and zero-filling grid points without observations. A more difficult issue is that we observe big performance gaps between training set and test set. Huracan's performance in a training year, 2017, drastically outperforms the metrics of both Huracan and Huracan-Hybrid in the test year of 2024 (not shown). More research is needed to find out the cause and potential solutions to this kind of overfitting.

Another point worth discussing is the inclusion of reanalysis (ERA5) as truth data. Using ERA5 as the optimization target for both the forecasting and assimilation models means that the training of Huracan is not independent of NWP-generated analysis, and therefore the system will learn some biases inherent in the original NWP. However, several features of our system help mitigate this, including the injection of noise and optimization of CRPS and the long auto-regressive fine-tuning which forces the model to produce more "correct" initial conditions that improve forecast accuracy at longer lead times. Once trained, Huracan is nevertheless a system which is able to run completely independently of NWP indefinitely.

We believe our work of ensemble assimilation and prediction offers a promising direction towards highly skillful and operational end-to-end data-driven weather prediction systems. Our data processing and training workflow can serve as the basis of further advancements that can potentially lead to comprehensive outperformance against the current state-of-the-art approach using initial conditions from NWP.

References

[1] Weyn, J.A., Durran, D.R., Caruana, R.: Can machines learn to predict weather? using deep learning to predict gridded 500-hpa geopotential height from historical weather data. Journal of Advances in Modeling Earth Systems **11**(8), 2680–2693 (2019)

[2] Bi, K., Xie, L., Zhang, H., Chen, X., Gu, X., Tian, Q.: Accurate medium-range

global weather forecasting with 3d neural networks. Nature **619**(7970), 533–538 (2023)

[3] Lam, R., Sanchez-Gonzalez, A., Willson, M., Wirnsberger, P., Fortunato, M., Alet, F., Ravuri, S., Ewalds, T., Eaton-Rosen, Z., Hu, W., *et al.*: Learning skillful medium-range global weather forecasting. Science **382**(6677), 1416–1421 (2023)

[4] Price, I., Sanchez-Gonzalez, A., Alet, F., Andersson, T.R., El-Kadi, A., Masters, D., Ewalds, T., Stott, J., Mohamed, S., Battaglia, P., Lam, R., Willson, M.: Probabilistic weather forecasting with machine learning. Nature **637**(8044), 84–90 (2025)

[5] Lang, S., Alexe, M., Clare, M.C.A., Roberts, C., Adewoyin, R., Bouallègue, Z.B., Chantry, M., Dramsch, J., Dueben, P.D., Hahner, S., Maciel, P., Prieto-Nemesio, A., O'Brien, C., Pinault, F., Polster, J., Raoult, B., Tietsche, S., Leutbecher, M.: AIFS-CRPS: Ensemble forecasting using a model trained with a loss function based on the continuous ranked probability score. arXiv preprint arXiv:2412.15832 (2024)

[6] Allen, A., Markou, S., Tebbutt, W., Requeima, J., Bruinsma, W.P., Andersson, T.R., Herzog, M., Lane, N.D., Chantry, M., Hosking, J.S., Turner, R.E.: End-to-end data-driven weather prediction. Nature **641**(8065), 1172–1179 (2025)

[7] Sun, X., Zhong, X., Xu, X., Huang, Y., Li, H., Neelin, J.D., Chen, D., Feng, J., Han, W., Wu, L., Qi, Y.: A data-to-forecast machine learning system for global weather. Nature Communications **16**(1), 6658 (2025)

[8] Alexe, M., Boucher, E., Lean, P., Pinnington, E., Laloyaux, P., McNally, A., Lang, S., Chantry, M., Burrows, C., Chrust, M., Pinault, F., Villeneuve, E., Bormann, N., Healy, S.: GraphDOP: Towards skilful data-driven medium-range weather forecasts learnt and initialised directly from observations. arXiv preprint arXiv:2412.15687 (2024)

[9] Magnusson, L., Chen, J.-H., Lin, S.-J., Zhou, L., Chen, X.: Dependence on initial conditions versus model formulations for medium-range forecast error variations. Quarterly Journal of the Royal Meteorological Society **145**(722), 2085–2100 (2019)

[10] Harrison, M.S.J., Palmer, T.N., Richardson, D.S., Buizza, R.: Analysis and model dependencies in medium-range ensembles: Two transplant case-studies. Quarterly Journal of the Royal Meteorological Society **125**(559), 2487–2515 (1999)

[11] Bannister, R.N.: A review of operational methods of variational and ensemble-variational data assimilation. Quarterly Journal of the Royal Meteorological Society **143**(703), 607–633 (2017)

[12] ECMWF: IFS Documentation CY48R1 - Part II: Data assimilation. IFS Documentation CY48R1 (2) (2023)

[13] Eyre, J.R., Bell, W., Cotton, J., English, S.J., Forsythe, M., Healy, S.B., Pavelin, E.G.: Assimilation of satellite data in numerical weather prediction. part ii: Recent years. Quarterly Journal of the Royal Meteorological Society **148**(743), 521–556 (2022)

[14] Dahoui, M., Isaksen, L., Radnoti, G.: Assessing the impact of observations using observation-minus-forecast residuals. ECMWF (2017). https://www.ecmwf.int/node/18195

[15] Healy, S., Bormann, N., Geer, A., Holm, E., Ingleby, B., Lean, K., Lonitz, K., Lupu, C.: Methods for assessing the impact of current and future components of the global observing system. ECMWF Technical Memoranda **916** (2024)

[16] NOAA: TIROS Operational Vertical Sounder (TOVS). (Accessed on 2025-08-13). https://www.aev.class.noaa.gov/saa/products/search?sub_id=0&datatype_family=TOVS

[17] EUMETSAT: AMSU-A Level 1B - Metop - Global. (Accessed on 2025-08-13). https://navigator.eumetsat.int/product/EO:EUM:DAT:METOP:AMSUL1

[18] AIRS project: AIRS/Aqua L1B AMSU (A1/A2) geolocated and calibrated brightness temperatures V005 (AIRABRAD). (Accessed on 2025-08-13) (2007). https://disc.gsfc.nasa.gov/datasets/AIRABRAD_005/summary

[19] EUMETSAT: MHS Level 1B - Metop - Global. (Accessed on 2025-08-13). https://navigator.eumetsat.int/product/EO:EUM:DAT:METOP:MHSL1

[20] Jet Propulsion Laboratory: Bjorn Lambrigtsen: Suomi NPP ATMS Sounder Science Investigator-led Processing System (SIPS) Level 1B Brightness Temperature V3 (SNPPATMSL1B). (Accessed on 2025-08-13) (2020). https://disc.gsfc.nasa.gov/datasets/SNPPATMSL1B_3/summary

[21] Jet Propulsion Laboratory: Bjorn Lambrigtsen: JPSS-1 ATMS Level 1B Brightness Temperature V3 (SNDRJ1ATMSL1B). (Accessed on 2025-08-13) (2020). https://disc.gsfc.nasa.gov/datasets/SNDRJ1ATMSL1B_3/summary

[22] NOAA: JPSS ATMS SDR Operational (ATMS_SDR). (Accessed on 2025-08-13). https://www.aev.class.noaa.gov/saa/products/search?sub_id=0&datatype_family=ATMS_SDR

[23] EUMETSAT: IASI Level 1C - All Spectral Samples - Metop - Global. (Accessed on 2025-08-13). https://navigator.eumetsat.int/product/EO:EUM:DAT:METOP:IASIL1C-ALL

[24] UW-Madison Space Science and Engineering Center: Hank Revercomb; UMBC Atmospheric Spectroscopy Laboratory: Larrabee Strow: Suomi NPP CrIS Level 1B Normal Spectral Resolution V3 (SNPPCrISL1BNSR). (Accessed on 2025-08-13) (2020). https://disc.gsfc.nasa.gov/datasets/SNPPCrISL1BNSR_3/summary

[25] UW-Madison Space Science and Engineering Center: Hank Revercomb; UMBC Atmospheric Spectroscopy Laboratory: Larrabee Strow: Suomi NPP CrIS Level 1B Full Spectral Resolution V3 (SNPPCrISL1B). (Accessed on 2025-08-13) (2020). https://disc.gsfc.nasa.gov/datasets/SNPPCrISL1B_3/summary

[26] UW-Madison Space Science and Engineering Center: Hank Revercomb; UMBC Atmospheric Spectroscopy Laboratory: Larrabee Strow: JPSS-1 CrIS Level 1B Full Spectral Resolution V3 (SNDRJ1CrISL1B). (Accessed on 2025-08-13) (2020). https://disc.gsfc.nasa.gov/datasets/SNDRJ1CrISL1B_3/summary

[27] UW-Madison Space Science and Engineering Center: Joe Taylor; UMBC Atmospheric Spectroscopy Laboratory: Larrabee Strow: JPSS-2 CrIS Level 1B Beta Full Spectral Resolution V3 (SNDRJ2CrISL1B). (Accessed on 2025-08-13) (2023). https://disc.gsfc.nasa.gov/datasets/SNDRJ2CrISL1B_3/summary

[28] AIRS project: AIRS/Aqua L1B Infrared (IR) geolocated and calibrated radiances V005 (AIRIBRAD). (Accessed on 2025-08-13) (2007). https://disc.gsfc.nasa.gov/datasets/AIRIBRAD_005/summary

[29] UCAR: Earth Radio Occultation. (Accessed on 2026-06-15). https://registry.opendata.aws/gnss-ro-opendata

[30] NOAA: NOAA Geostationary Operational Environmental Satellites (GOES) 16, 17, 18 & 19. (Accessed on 2025-08-13). https://registry.opendata.aws/noaa-goes/

[31] NOAA and JMA: JMA Himawari-8/9. (Accessed on 2025-08-13). https://registry.opendata.aws/noaa-himawari/

[32] EUMETSAT: High Rate SEVIRI Level 1.5 Image Data - MSG - 0 degree. (Accessed on 2025-08-13). https://navigator.eumetsat.int/product/EO:EUM:DAT:MSG:HRSEVIRI

[33] EUMETSAT: High Rate SEVIRI Level 1.5 Image Data - MSG - Indian Ocean. (Accessed on 2025-08-13). https://navigator.eumetsat.int/product/EO:EUM:DAT:MSG:HRSEVIRI-IODC

[34] Knapp, K.R., Wilkins, S.L.: Gridded satellite (GridSat) GOES and CONUS data. Earth System Science Data **10**(3), 1417–1425 (2018)

[35] Knapp, K.R., Ansari, S., Bain, C.L., Bourassa, M.A., Dickinson, M.J., Funk, C., Helms, C.N., Hennon, C.C., Holmes, C.D., Huffman, G.J., Kossin, J.P., Lee, H.-T., Loew, A., Magnusdottir, G.: Globally gridded satellite observations for climate

studies. Bulletin of the American Meteorological Society **92**(7), 893–907 (2011)

[36] Durre, I., Yin, X., Vose, R.S., Applequist, S., Arnfield, J., Korzeniewski, B., Hundermark, B.: Integrated Global Radiosonde Archive (IGRA), Version 2. NOAA National Centers for Environmental Information. (Accessed on 2025-08-13) (2016). https://doi.org/10.7289/V5X63K0Q

[37] NOAA NCEI: Global Hourly - Integrated Surface Database (ISD). (Accessed on 2025-08-13). https://www.ncei.noaa.gov/products/land-based-station/integrated-surface-database

[38] Hersbach, H., Bell, B., Berrisford, P., Hirahara, S., Horányi, A., Muñoz-Sabater, J., Nicolas, J., Peubey, C., Radu, R., Schepers, D., *et al.*: The ERA5 global reanalysis. Quarterly Journal of the Royal Meteorological Society **146**(730), 1999–2049 (2020)

[39] Bonev, B., Kurth, T., Hundt, C., Pathak, J., Baust, M., Kashinath, K., Anandkumar, A.: Spherical fourier neural operators: learning stable dynamics on the sphere. In: Proceedings of the 40th International Conference on Machine Learning. ICML'23 (2023)

[40] Liu, Z., Lin, Y., Cao, Y., Hu, H., Wei, Y., Zhang, Z., Lin, S., Guo, B.: Swin transformer: Hierarchical vision transformer using shifted windows. In: Proceedings of the IEEE/CVF International Conference on Computer Vision, pp. 10012–10022 (2021)

[41] Ni, Z.: Kunyu: A high-performing global weather model beyond regression losses. arXiv preprint arXiv:2312.08264 (2023)

[42] Chen, M., Tan, X., Li, B., Liu, Y., Qin, T., Zhao, S., Liu, T.-Y.: AdaSpeech: Adaptive text to speech for custom voice. arXiv preprint arXiv:2103.00993 (2021)

[43] Berre, L.: Simulation and diagnosis of observation, model and background error contributions in data assimilation cycling. Quarterly Journal of the Royal Meteorological Society **145**(719), 597–608 (2019)

[44] ECMWF: IFS Documentation CY48R1 - Part V: Ensemble prediction system. IFS Documentation CY48R1 (5) (2023)

A Implementation Details

A.1 Hyperspectral Infrared and Radio Occultation Embeddings

A.1.1 Input Preparation

Hyperspectral Infrared

CrIS spectrums are first apodized to match the processing level of IASI. All hyperspectral infrared spectrums are then converted to brightness temperatures and upsampled to a resolution of 0.125 cm^{-1}, with 16,921 channels in total.

Radio Occultation

Bending angle profiles from radio occultations are interpolated to 999 pressure-altitude levels from 0.001 atm to 0.999 atm. After that, six features are computed at each level, including bending angle, coordinate difference from the nearest grid point, and angle of orientation. Those features are concatenated together to yield 5,994 channels in total.

A.1.2 Autoencoder Training

Two simple multi-layer perceptron (MLP) autoencoders are separately trained to compress the thousands of channels from each observation category. The two autoencoders both consist of a 4-layer encoder and a 4-layer decoder, with the size of bottleneck equal to the number of embedding dimensions (32 in hyperspectral IR, 64 in radio occultation), and are trained to minimize the L1 loss of the reconstructed spectrum. When missing channels are present, such as in the cases of data coming from instruments other than IASI, or partial occultations that do not reach the ground, those unobserved channels are set to -5 after normalization. The encoders are then used to compress hyperspectral infrared and radio occultation observations into their desired number of channels to be used in Huracan. Figure 7 shows an example of hyperspectral infrared spectrum reconstruction by its autoencoder.

A.2 SFNO Filter Compression

In the original implementation of SFNO, There is one separate linear filter $\tilde{\kappa}_\vartheta(l)$ associated with each degree $0 \leq l \leq L$. This brute-force implementation ignores the fact that adjacent zonal modes should be more related to each other.

In our work, we encode each degree l with a sinusoidal encoding, forging connections between adjacent degrees. This encoding is then concatenated with the noise embeddings for noise injection, and transformed by a MLP into a k-dimensional embedding $h(l)$. The filter weight for this l is in turn constructed by computing the weighted sum of learned filter weights of each embedding dimension $\tilde{\kappa}_i$:

$$\kappa(l) = \sum_{i=1}^{k} h_i(l)\tilde{\kappa}_i.$$

Therefore, there are only k learnable linear filters instead of $L + 1$ linear filters. In our model, 1-degree resolution implies $L = 179$. Setting $k = 15$ results in a 12-fold reduction on the number of parameters.

A.3 Training Parameters

We use a batch size of 16 for all experiments and an ensemble size of 2 for training all stochastic models. Table 3 lists more training parameters in all training stages.

Table 3: Training settings for Huracan.

Training Target	Data	Max. LR	Schedule	#Steps
Deterministic base model	1979-2014 ERA5	5e-4	cosine	347k
Stochastic base model	1979-2014 ERA5	2e-4	cosine	149k
Initial forecasting model	1979-2014 ERA5	3e-6	constant	14k
Initial assimilation model	2010-2022 ERA5+Obs.	2e-4	cosine	46k
Final Huracan models	2010-2022 ERA5+Obs.	3e-6	cosine	13k
Huracan-Hybrid	2018-2022 ECMWF HRES	3e-6	constant	2.7k

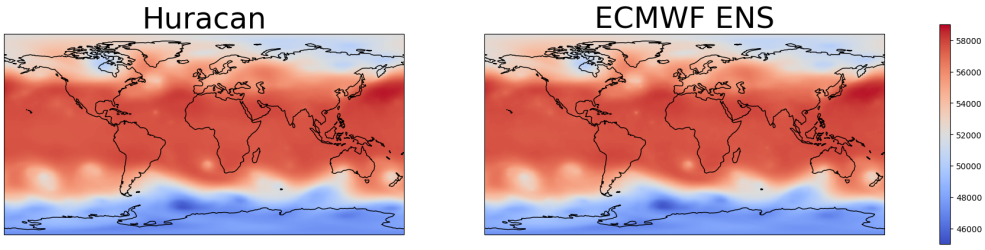

(a) Ensemble mean of 500 hPa geopotential (m^2/s^2)

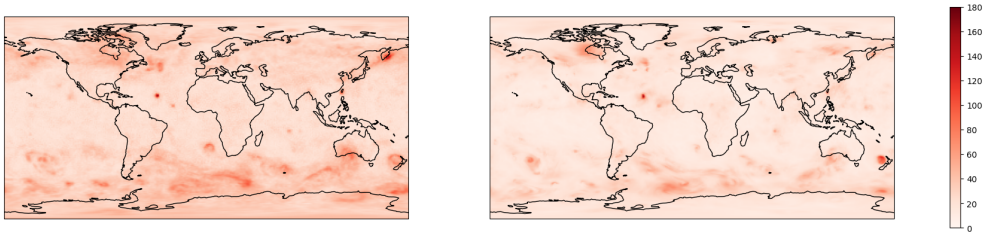

(b) Ensemble standard deviation of 500 hPa geopotential (m^2/s^2)

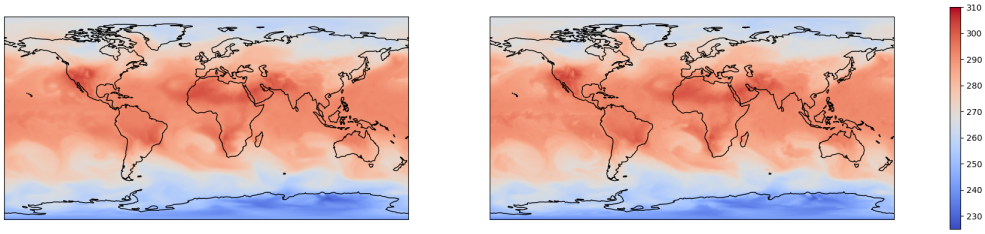

(c) Ensemble mean of 850 hPa temperature (K)

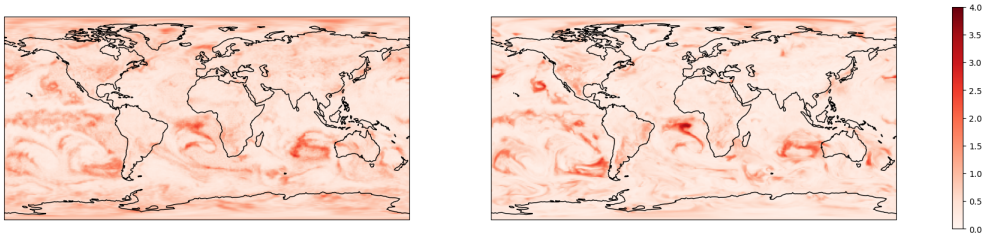

(d) Ensemble standard deviation of 850 hPa temperature (K)

Fig. 6: **Visualizations of ensemble statistics.** Plots shown above are ensemble mean and standard deviation of two vital atmospheric variables, 500 hPa geopotential and 850 hPa temperature, from Huracan and ECMWF ENS initial conditions at 0 UTC on October 3, 2024.

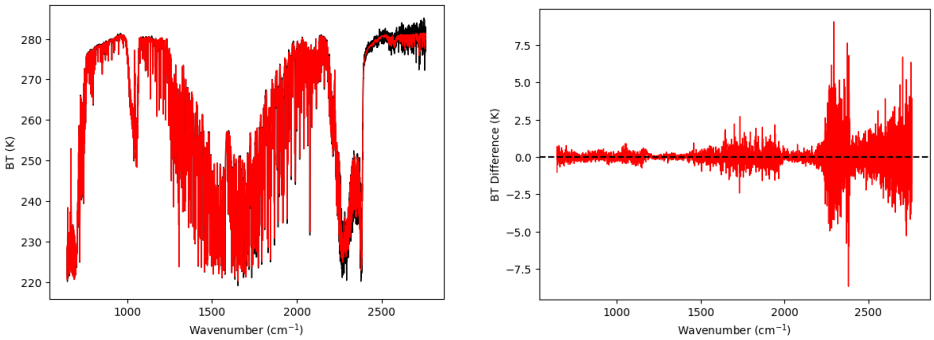

(a) (b)

Fig. 7: **A reconstruction example of our hyperspectral IR autoencoder.** (a) The original IASI spectrum (black) versus our reconstructed spectrum (red). The two lines mostly overlap with each other. (b) Difference of brightness temperatures (BT) between the original spectrum and our reconstruction. The reconstruction quality is poorer in the shortwave section where there is more instrument noise.